JACS
JOURNAL OF THE AMERICAN CHEMICAL SOCIETY
Article
Cite This: J. Am. Chem. Soc. 2018, 140, 5791−5797
pubs.acs.org/JACS

Nanoporous Copper−Silver Alloys by Additive-Controlled Electrodeposition for the Selective Electroreduction of CO_2 to Ethylene and Ethanol

Thao T. H. Hoang,[†,#,⊗] Sumit Verma,[‡,§] Sichao Ma,[†,§] Tim T. Fister,[⊥] Janis Timoshenko,[∥] Anatoly I. Frenkel,[∥] Paul J. A. Kenis,[‡,§] and Andrew A. Gewirth*[,†,§]

[†]Department of Chemistry, University of Illinois at Urbana−Champaign, Urbana, Illinois 61801, United States
[‡]Department of Chemical & Biomolecular Engineering, University of Illinois at Urbana−Champaign, Urbana, Illinois 61801, United States
[§]International Institute for Carbon Neutral Energy Research (WPI-I2CNER), Kyushu University, Fukuoka 819-0385, Japan
[⊥]Chemical Sciences and Engineering Division, Argonne National Laboratory, Argonne, Illinois 60439, United States
[∥]Department of Materials Science and Chemical Engineering, Stony Brook University, Stony Brook, New York 11794, United States
[#]Graduate University of Science and Technology, Vietnam Academy of Science and Technology, Hanoi, Vietnam
[⊗]Institute of Chemistry, Vietnam Academy of Science and Technology, Hanoi, Vietnam

Supporting Information

ABSTRACT: Electrodeposition of CuAg alloy films from plating baths containing 3,5-diamino-1,2,4-triazole (DAT) as an inhibitor yields high surface area catalysts for the active and selective electroreduction of CO_2 to multicarbon hydrocarbons and oxygenates. EXAFS shows the co-deposited alloy film to be homogeneously mixed. The alloy film containing 6% Ag exhibits the best CO_2 electroreduction performance, with the Faradaic efficiency for C_2H_4 and C_2H_5OH production reaching nearly 60 and 25%, respectively, at a cathode potential of just −0.7 V vs RHE and a total current density of ∼ − 300 mA/cm^2. Such high levels of selectivity at high activity and low applied potential are the highest reported to date. *In situ* Raman and electroanalysis studies suggest the origin of the high selectivity toward C_2 products to be a combined effect of the enhanced stabilization of the Cu_2O overlayer and the optimal availability of the CO intermediate due to the Ag incorporated in the alloy.

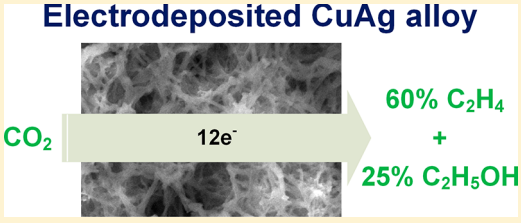

1. INTRODUCTION

Carbon dioxide (CO_2) emissions, mostly as the result of human activities involving combustion (burning) of fossil fuels for electricity, heat, and transportation, have increased exponentially.[1] Elevated levels of CO_2 in the atmosphere have been linked to many serious environmental threats, including but not limited to global warming, rising sea levels, and more erratic weather patterns.[2] Proposed methods for decreasing the levels of CO_2 in the atmosphere involve capturing and sequestering CO_2 underground or underwater,[3,4] or converting it to value-added chemicals.[3,5−7] A way to minimize CO_2 emissions could be to utilize clean renewable energy sources such as wind and solar, which are attracting increased attention. However, renewable energy output and energy consumption are intermittent, thus requiring efficient energy conversion and storage systems to be coupled to energy generation. A promising approach to both mitigate CO_2 levels and utilize excess electricity from renewable sources would be to electrochemically reduce CO_2 to value-added chemicals or fuels.[8−10]

The pioneering work of Hori et al. in the early 1990s showed Cu to be the only transition metal CO_2 electroreduction catalyst that could produce multicarbon hydrocarbons and oxygenates such as ethylene (C_2H_4) and ethanol (C_2H_5OH), albeit at low levels of activity (−5 mA/cm^2) and selectivity (i.e., the Faradaic efficiency, FE, for C_2H_4 and C_2H_5OH was 25.5% and 5.7%, respectively).[10] Since then, several studies have focused on changing the composition and morphology of Cu-based catalysts to tune and ideally improve the selectivity and activity of CO_2 electroreduction toward multicarbon products.[9−24] For example, Cu_2O or Cu_2O-derived Cu catalysts have been extensively reported to enhance the electroreduction of CO_2 to C_2 products such as C_2H_4 and C_2H_5OH.[13−15,17] Single-crystal Cu electrodes such as Cu[100][25] or Cu[100] terraces with Cu[111] or Cu[110] steps have been reported to promote C_2H_4 formation.[26] More recently, Cu-based bimetallics have emerged as another class of CO_2 electroreduction catalysts that can enhance the selectivity of CO_2 electroreduction toward different products by modulating the adsorption of key intermediates on the catalyst surface. For instance, enhancements in the activity and selectivity for CO

Received: February 14, 2018
Published: April 5, 2018

DOI: 10.1021/jacs.8b01868
J. Am. Chem. Soc. 2018, 140, 5791−5797

have been observed on bimetallic CuAg[20] and CuAu,[21,22] for formic acid on CuSn and CuPb,[27] and for C_2H_5OH on CuZn.[19] Furthermore, compressively strained CuAg bimetallics have been shown to improve the selectivity of CO_2 electroreduction toward multicarbon oxygenates.[28] However, even after such extensive research efforts, achieving high selectivity (FE $\gg$ 50%) for C_2 products (C_2H_4 and C_2H_5OH) at high activity (current density $\ll -200$ mA/cm^2) while requiring low energy input (applied potential $\gg -1.0$ V vs RHE), requirements for any industrially interesting process,[29,30] remains a major challenge in the field.[31]

In this work, we focus on enhancing the selectivity of CO_2 electroreduction toward C_2 products such as C_2H_4 and C_2H_5OH. A bimetallic CuAg catalyst (prepared using additive-controlled electrodeposition) with a nanoporous structure and low Ag content (<10%) is reported. The CuAg catalyst exhibits high selectivity toward C_2H_4 (~60%) and C_2H_5OH production (~25%) at a relatively low applied potential (−0.7 V vs RHE) and a high current density (−300 mA/cm^2) for the electroreduction of CO_2 in an alkaline flow electrolyzer. These results represent a major improvement in performance over the state-of-the-art Cu-based catalysts for the production of C_2H_4 (plasma-activated Cu: FE ~60% at −0.9 V vs RHE and current density ~ −20 mA/cm^2 evaluated in a two-compartment cell with dissolved CO_2 as the feed and 0.1 M $KHCO_3$ as the electrolyte under static conditions,[17] and Cu nanoparticles: FE ~35% at −0.6 V vs RHE evaluated in a gas diffusion electrode-based flow electrolyzer with a continuous supply of CO_2 at the electrode−electrolyte interface and 1 M KOH as the electrolyte under flowing conditions)[13] as well as C_2H_5OH (Cu_xZn: FE ~29.1% at −1.05 V vs RHE and current density ~ −30 mA/cm^2 evaluated in a static two-compartment cell with 0.1 M $KHCO_3$ as the electrolyte,[19] and Cu nanoparticles: FE ~17% at −0.8 V vs RHE evaluated in the flow electrolyzer with 1 M KOH as the electrolyte).[13] Using the combination of *in situ* Raman and a series of control experiments, we further show that the enhanced selectivity toward C_2H_4 and C_2H_5OH can be attributed to the stabilization of the Cu_2O overlayer and the optimal availability of the CO intermediate (key for C−C coupling) due to the added Ag.

2. EXPERIMENTAL SECTION

2.1. Preparation of Catalysts. Cu and CuAg samples were electrodeposited in a plating bath made from 0.1 M $CuSO_4 \cdot 5H_2O$ + 10 mM 3,5-diamino-1,2,4-triazole (DAT), with or without 1 mM Ag_2SO_4, at pH = 1.5 adjusted by using H_2SO_4. All chemicals were obtained from Sigma-Aldrich. Cu was electrodeposited galvanostatically at a constant current density of 4 mA/cm^2 until a final deposition charge of 2 C/cm^2 was reached (unless stated otherwise). Pt wire was used as the counter electrode, separated from the working electrode by an ion exchange membrane (Fumatech FAP-375-PP) in a two-compartment electrochemical cell to avoid oxidation of the additives. A "leakless" Ag/AgCl (eDAQ) electrode was placed near the working electrode to measure the potential. The substrates for electrodeposition were cleaned or pretreated just before use.

For the CO_2 electroreduction measurements in a flow electrolyzer, Cu and CuAg were electrodeposited on carbon paper and used as a gas diffusion electrode.[32] Carbon paper (GDL, Sigracet 35 BC, Ion Power) was either activated by immersion in concentrated HNO_3 for 1 h or electron-beam-coated with ~10 nm of Cu (~0.01 mg/cm^2) before the electrodeposition step. Carbon paper pretreated by both methods exhibited similar morphology and electrochemical activity. However, the HNO_3 treatment made both sides of the carbon paper hydrophilic, allowing liquid transport through the paper, which occasionally resulted in the flooding of the electrolyte into the gas chamber. Thus, the carbon paper coated with Cu was used as the substrate, with 2 C/cm^2 of Cu or CuAg electrodeposited onto the 1 × 2.5 cm^2 section of the coated carbon paper.

2.2. Materials Characterization. The amount of electrodeposited Cu and Ag was measured using inductively coupled plasma optical emission spectrometry (ICP-OES; PerkinElmer 2000 DV optical emission spectrometer). Scanning electron microscopy (SEM) images were obtained using a Hitachi A-4700 high-resolution microscope. X-ray photoelectron spectroscopy (XPS) was performed with a Physical Electronics PHI 5400 instrument. The %Ag in the CuAg samples was measured using energy-dispersive spectroscopy (EDS) during SEM and by using XPS. Results from ICP-OES, EDS, and XPS agreed to within 2%.

X-ray absorption spectroscopy was carried out at sector 9 beamline (BM) at the Advanced Photon Source at Argonne National Laboratory with a beam cross section of 2.6 × 0.75 mm. Samples were studied *ex situ* by layering 12 sheets of carbon paper electrodeposited with the sample. All measurements were recorded in transmission mode using a double-crystal Si (111) monochromator run at 50% detuning and ion chamber detectors filled with a mixture of He/N_2.

Pb underpotential deposition (UPD) was used to determine the electroactive surface areas.[33] Measurements were obtained from electrodeposits on both Au and carbon paper. While the results were similar between the two substrates, the error in repeated measurements was higher using the carbon paper relative to the Au substrate, presumably due to the smoother and more reproducible surface presented by the freshly flamed Au.

2.3. CO_2 Electroreduction in a Flow Electrolyzer. Electrochemical measurements and product detection were conducted in a flow electrolyzer setup described previously.[13] The activity of each catalyst for CO_2 electroreduction was measured by controlling the cell potential (−1.6, −1.75, −2.0, −2.25, −2.5, −2.75, −3, and −3.5 V) using an Autolab PGSTAT-30, EcoChemie potentiostat. The electrolyte was 1 M KOH. Cathode potentials were reported with respect to the reversible hydrogen electrode (RHE): E (vs RHE) = E (vs Ag/AgCl) + 0.209 V + 0.0591 V/pH × pH − η_{IRdrop}. The gaseous product stream was sampled automatically and diverted and analyzed in a gas chromatograph (Thermo Finnigan Trace GC) equipped with both a thermal conductivity detector (TCD) and a flame ionization detector (FID). The exit electrolyte containing liquid products was collected and analyzed using a ^{1}H NMR technique as described previously.[13] For regular CO_2 electroreduction experiments, the CO_2 flow rate was set at 7 SCCM. For CO_2 reduction experiments in the presence of CO, the flow rates for CO_2 and CO were 7 SCCM and 1 SCCM, respectively.

2.4. *In Situ* Electrochemical Raman Measurements. *In situ* Raman measurements were conducted using a spectroelectrochemical flow cell adapted from the cell described previously.[34] For Raman experiments, the working electrodes were Cu or CuAg samples electrodeposited on a carbon paper. The counter electrode was a Pt wire and the reference electrode was Ag/AgCl, which was calibrated before each experiment with a normal hydrogen electrode in 1 M $HClO_4$. A syringe pump (PHD 2000, Harvard Apparatus) was used to flow the electrolyte through the cell to minimize boundary layer depletion effects and supply fresh electrolyte, thereby helping to maintain constant pH at the electrode surface. The flow rate of the 1 M KOH electrolyte was set at 20 mL/min. The pH of the electrolyte was measured using a calibrated pH meter (Thermo Orion, 9106BNWP). CO_2 gas was introduced into the cell through the back side of the carbon paper working electrode at a flow rate of 4 SCCM. Potentials are reported with respect to the RHE. For each *in situ* Raman experiment, the potential was held at −0.7 V, and the Raman spectrum was acquired from 30 1-s acquisitions.

3. RESULTS AND DISCUSSION

3.1. Characterization of Cu Films. Cu and bimetallic CuAg samples with various quantities of Ag dopant were prepared by electrodeposition with and without the presence of

DOI: 10.1021/jacs.8b01868
J. Am. Chem. Soc. 2018, 140, 5791−5797

DAT as an electrodeposition additive. Previously, we showed that electrodeposition of Cu in the presence of DAT at pH = 1.5 leads to a wire-like morphology for the Cu deposit, as shown in Figure 1a. We wondered how added Ag might change

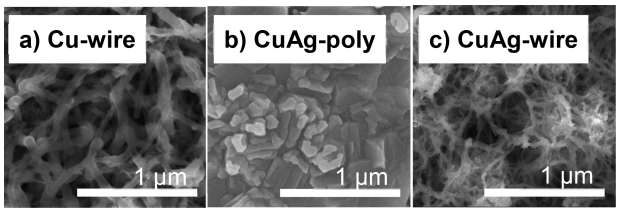

Figure 1. SEM of (a) Cu wire (0% Ag) electrodeposited with DAT, (b) CuAg poly (6% Ag) electrodeposited without DAT, and (c) CuAg wire (6% Ag) electrodeposited with DAT.

the deposit morphology. Figure 1b shows a CuAg film (CuAg poly) containing 6% Ag (as measured by ICP-OES) deposited without DAT in solution. The film exhibits large particles, similar to deposits reported previously.[35]

Addition of DAT to the CuAg plating bath leads to a different morphology. Figure 1c shows the CuAg wire deposit containing 6% Ag (as measured by ICP-OES). The image shows the presence of wire-like deposits exhibiting substantial porosity.[32,36] The wires are approximately a factor of 2 smaller in diameter relative to the deposit formed from Cu alone. Deposits made from different amounts of Ag also exhibited structures similar to those found in Figure 1c (see also Figure S1).

Figure 2 shows XRD patterns obtained from CuAg poly (6% Ag) electrodeposited without DAT, Cu wire (0% Ag)

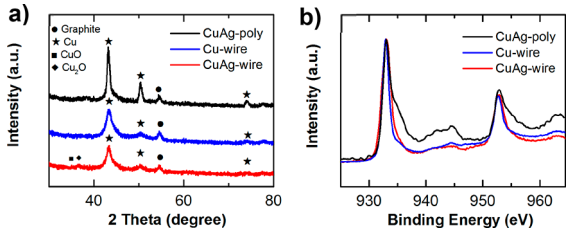

Figure 2. (a) XRD and (b) XPS patterns of CuAg poly (6% Ag) electrodeposited without DAT, Cu wire (0% Ag) electrodeposited with DAT, and CuAg wire (6% Ag) electrodeposited with DAT.

electrodeposited with DAT, and CuAg wire (6% Ag) electrodeposited with DAT. The XRD shows the presence of mostly metallic Cu with Cu peaks at 2θ = 43.46° (from Cu (111)), 50.62° (from Cu (200)), and 74.40° (from Cu (220)). No Ag-related peaks are found, due to the relatively small amount of Ag present.[37] The CuAg wire sample also exhibits a small peak at 2θ = 36.95° associated with the presence of Cu_2O. The Cu peaks in the XRD patterns of CuAg wire and Cu wire samples are broader and less intense than those found in the Cu poly sample, indicating that CuAg wire and Cu wire samples exhibit a smaller crystallite size than Cu poly. The crystallite sizes of CuAg poly, Cu wire, and CuAg wire samples calculated from XRD patterns using the Scherer equation are 21.1, 4.6, and 3.7 nm, respectively, as given in Table 1.

Figure 2b shows the XPS patterns obtained from the CuAg poly, Cu wire, CuAg wire samples. While Cu wire and CuAg wire show only two peaks associated with Cu (0), the CuAg poly material exhibits a series of satellite peaks[38−40] from CuO,

Table 1. Parameters Obtained from Cu and CuAg Samples

	$\frac{A_{active}}{A_{geometric}}$	crystalline size (nm)	loading (mg/cm^2)
CuAg poly (6% Ag)	~1.3	~21.1	~0.5
Cu wire	~7.3	~4.6	~0.3
CuAg wire (6% Ag)	~8.1	~3.6	~0.3

suggesting that CuAg poly contains more oxide (at least on the surface) than the others. While the XRD reported on the presence of Cu_2O for the CuAg wire sample, peaks associated with Cu(I) are difficult to distinguish from those for Cu(0) in XPS.[38,39]

The electroactive surface area of the different Cu and CuAg samples was measured by using Pb UPD to form a conformal Pb coating on the accessible part of the Cu deposit.[33,41] The results (Table 1) show that the CuAg sample electrodeposited without DAT exhibits an electroactive surface area similar to the geometric area, as expected due to the large particles seen in the SEM. Alternatively, the Cu wire and CuAg wire (6%) samples exhibit electroactive surface area 7−8 times larger than the geometric area. CuAg wire exhibits ~10% larger surface area than the Cu samples (Figure 1 and Table 1).

Cu and Ag K-edge EXAFS spectra and analysis (Figure 3 and Table 2) were utilized to determine the local bonding

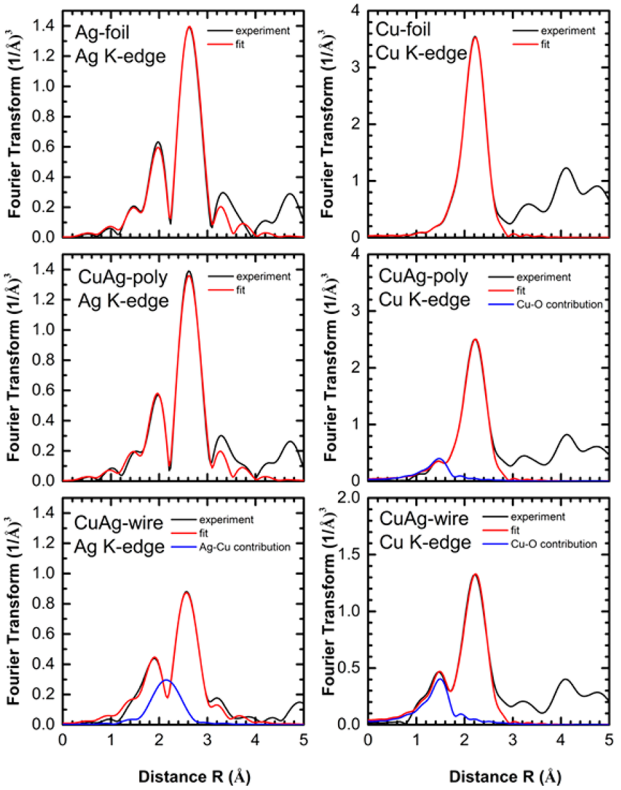

Figure 3. Best fit for Ag K-edge and Cu K-edge EXAFS data for CuAg wire and CuAg poly samples and Cu and Ag foils: Fourier transforms (FTs) for experimental and modeled EXAFS data.

environment of Cu and Ag in the samples containing Ag. The data show that both CuAg wire (6%) and CuAg poly (6%) samples appear to be mostly metallic since Fourier transforms (FT) of the EXAFS spectra for CuAg samples are similar to those for the corresponding metallic foil.

DOI: 10.1021/jacs.8b01868
J. Am. Chem. Soc. 2018, 140, 5791−5797

Table 2. Values of Structural Parameters for the First Coordination Shell of Cu and Ag Atoms in CuAg Wire and CuAg Poly Samples, Obtained from the Fits of Cu K-Edge and Ag K-Edge EXAFS Data

	Ag foil	Cu foil	CuAg wire (6%)	CuAg poly (6%)
ΔE_0 (eV), Ag K-edge	−8.6(1)		−10.2(4)	−8.8(1)
ΔE_0 (eV), Cu K-edge	−1.1(4)		0.5(6)	−0.4(5)
N_{Ag-Ag}	12		11.0(4)	12
N_{Ag-Cu}			2.0(6)	0
N_{Cu-Cu}		12	4.6(2)	8.6(4)
N_{Cu-O}			0.8(1)	0.4(2)
$\langle R\rangle_{Ag-Ag}$ (Å)	2.864(1)		2.822(6)	2.858(2)
$\langle R\rangle_{Ag-Cu}$ (Å)			2.641(7)	
$\langle R\rangle_{Cu-Cu}$ (Å)		2.537(2)	2.542(4)	2.540(4)
$\langle R\rangle_{Cu-O}$ (Å)			1.87(1)	1.85(2)
σ^2_{Ag-Ag} (Å^2)	0.0104(2)		0.0156(8)	0.0106(1)
σ^2_{Ag-Cu} (Å^2)			0.011(4)	
σ^2_{Cu-Cu} (Å^2)		0.0086(2)	0.0087(5)	0.0086(4)
σ^2_{Cu-O} (Å^2)			0.003(2)	0.003(5)

For CuAg poly (6%) samples, the contribution of Ag−Cu bonds to the total EXAFS spectra is not significant and cannot be detected within the uncertainties of our analysis (Figure 3). The structure parameters of CuAg poly (6%) (Table 2) that characterize the environment around Ag, as well as the ΔE_0 parameter that characterizes the electronic state of Ag atoms within error agree with those for bulk Ag material. Similarly, the average interatomic distances of Cu−Cu are the same as in bulk copper metal. These findings indicate that Cu and Ag atoms are completely segregated in the CuAg poly (6%) samples.

CuAg wire (6%), in turn, exhibits Ag−Cu bonds (Figure 3) with distance values between those for pure Cu and pure Ag (Table 2), as expected for alloys. Also, the Ag−Ag distance is slightly reduced in the CuAg wire sample, suggesting at least partial alloying of Ag atoms with smaller Cu atoms. The average interatomic distance for Cu−Cu is close to that in bulk material, which is reasonable considering the large amount of Cu relative to Ag in the CuAg wire (6%) samples.

Figure 3 shows that both CuAg wire (6%) and CuAg poly (6%) appear to be partially oxidized EXAFS fitting results (Figure 3 and Table 2) suggest the presence of Cu(I) oxide. The Cu−O distance of 1.85−1.87 Å is consistent with Cu−O distance in Cu_2O reported previously.[42] Note that CuAg wire (6%) appears to contain more Cu_2O than CuAg poly (6%). These EXAFS data are consistent with the XRD data (Figure 2), in which Cu_2O peak appears in XRD of CuAg wire (6%) but not of CuAg poly (6%).

The presence of CuO in CuAg samples (especially CuAg poly (6%)), which is evidenced in XPS spectra, is not observed in both EXAFS and XRD data. These results suggest that CuO might occur as a thin native oxide layer that forms on top of the CuAg sample in the atmosphere.

It is certainly possible that small amounts of Ag^+ are incorporated in the Cu_2O lattice. However, the presence of Ag^+ would lead to an exchange reaction producing Ag(0) and Cu(II)O. There is no evidence from either Raman or EXAFS to support or exclude presence of Ag^+.

3.2. CO_2 Electroreduction in a Flow Electrolyzer. To evaluate the catalytic activity and the product distribution for the electroreduction of CO_2 on the Cu and CuAg samples, we tested the materials in a flow electrolyzer. Figures 4 and 5 show the Faradaic efficiency and partial current density for CO_2

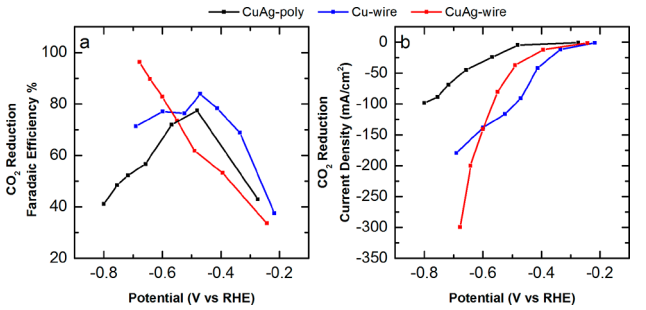

Figure 4. Faradaic efficiency and current density (normalized to the geometric area) for the electroreduction of CO_2 on the CuAg poly (black), Cu wire (blue), and CuAg wire (red) samples.

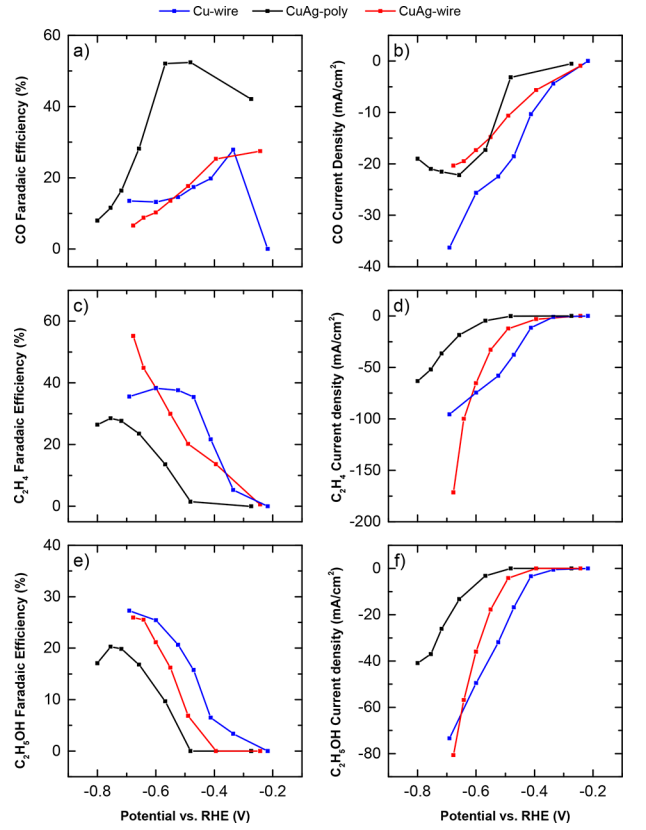

Figure 5. Faradaic efficiency and partial current density (normalized to the geometric area) for (a,b) CO production, (c,d) C_2H_4 production, and (e,f) C_2H_5OH production. Errors are ca. ±5%.

electroreduction as well as all the major products (CO, C_2H_4, and C_2H_5OH) obtained using CuAg poly (6%) electrodeposited without DAT, Cu wire (0% Ag) electrodeposited with DAT, and CuAg wire (6% Ag) electrodeposited with DAT in a 1 M KOH electrolyte as a function of cathode potential.

Figure 4a,b shows that the Cu wire and CuAg wire (6%) electrodeposited with DAT exhibit ∼5−6 times higher CO_2 electroreduction current density relative to CuAg poly (6%) electrodeposited without DAT. This enhancement in activity can be explained by the differences in their surface areas (Table 1). In particular, the CO_2 electroreduction current density values for CuAg poly, Cu wire, and CuAg wire at ∼ −0.7 V vs RHE are ∼ −50 mA/cm^2, ∼ −180 mA/cm ^{2}, and ∼ −300 mA/

DOI: 10.1021/jacs.8b01868
J. Am. Chem. Soc. 2018, 140, 5791−5797

cm^2, respectively. Interestingly, while the active surface area of CuAg wire is only ~10% higher than that of Cu wire (Table 1), the current density for CuAg wire (6%) is ~60% higher than that obtained from the Cu wire. This phenomenon suggests that differences in active surface area are not the only reason for the enhancement in CO_2 electroreduction activity between Cu wire and CuAg wire.

Figure 5a,b shows, that for all catalysts, CO formation starts at ~ −0.2 V vs RHE. The FE for CO production decreases with increasing FEs associated with C_2 products including C_2H_4 (Figure 5c,d) and C_2H_5OH (Figure 5e,f). A possible explanation for this trend is that adsorbed CO is an important intermediate for the formation of C_2 products, as has been suggested previously.[9,10,13,43−45]

Figure 5c−f shows that CuAg poly samples exhibit the lowest Faradaic efficiency and current density for C_2 formation relative to those obtained from Cu wire and CuAg wire samples, which probably can be explained by the effect of "nanosize" Cu wire and CuAg wire particles. The nanoporous surfaces of Cu wire and CuAg wire give rise to steps and edges with low-coordinated metal atoms, which have been postulated to be more active toward the reduction of CO_2 to C_2 products: steps and edges promote adsorption of C_1 intermediates and facilitate their dimerization to form C_2 products.[10,11,44,46−48]

Figure 5c−f also shows that both Cu wire and CuAg wire exhibit high Faradaic efficiency and current density for C_2 formation. While Cu wire samples reach 40% FE for C_2H_4 and 20% FE for C_2H_5OH at relatively low potential (~ −0.5 V vs RHE), the FE is maintained at this level even at more negative potentials. On the other hand, the CuAg wire sample reaches the same FE at ~ −0.6 V vs RHE and the FE continuously increases with increasing negative potential. Consequently, at high negative potential, CuAg wire exhibits higher activity and selectivity for C_2H_4 than those obtained from Cu wire. Particularly, at ~ −0.7 V vs RHE, the FE for C_2H_4 formation from CuAg wire (~60%) is higher than that of Cu wire (~40%), and the current density for C_2H_4 of CuAg wire (~ −180 mA/cm^2) is approximately a factor of 2 higher than that obtained from Cu wire (~ −90 mA/cm^2).

Further, we also evaluated the effect of CO addition on the efficacy of ethylene production. Figure 6 shows the effect of

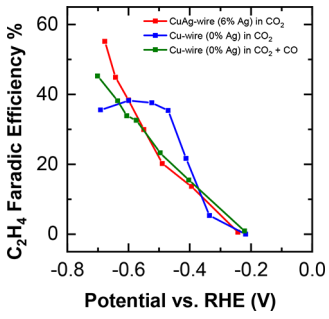

Figure 6. Faradaic efficiencies for C_2H_4 production from Cu wire and CuAg wire in CO_2 and CO_2 + CO. Errors are ca. ±5%.

adding CO (1 SCCM) to the CO_2 feed. The graph shows that while the added CO inhibits C_2H_4 production at low potentials, at high potentials added CO promotes the formation of C_2H_4, yielding a Cu wire catalyst only slightly worse than that presented by the CuAg wire electrode.

The Cu wire catalyst reaches 40% FE for C_2H_4 at relatively low potential (~ −0.5 V vs RHE), and the FE is maintained at this level even at more negative potentials (Figure 5). This saturation region of the C_2H_4 FE from the Cu wire catalyst is probably due to the lack of adsorbed CO due to the high turnover rate on the Cu wire electrode surface at more negative potentials. When CO is fed into the system during CO_2 reduction (Figure 6), the saturation region for C_2H_4 production from the Cu wire catalyst disappears.

HER suppression due to compressive strain from incorporation of Ag (≥20%) into the Cu surface,[49] and due to surface mesostructuring,[50,51] has been suggested to be a possible origin of enhanced selectivity for multicarbon products such as ethylene. However, in our CuAg wire catalyst the Ag content is only 6%. At this low value, compressive strain is likely not present in our alloy, and indeed there is no change in position of the primary reflections in the Cu XRD. Mesostructuring is also not likely to be an origin of the enhancement of ethylene production from CuAg wire. In particular, the mesostructured surfaces of both CuAg wire and Cu wire catalysts are quite similar (similar active surface area and similar morphology), but they exhibit significantly different activity. Also, current density and Faradaic efficiencies for H_2 production from Cu poly, Cu wire, and CuAg wire (Figure S3) are not remarkably different. This result shows that the improved FE for ethylene from CuAg wire is not due to HER suppression.

3.3. *In Situ* Raman Spectroscopy. Figure 7 reports *in situ* Raman spectra obtained in a flow cell utilizing an electrolyte

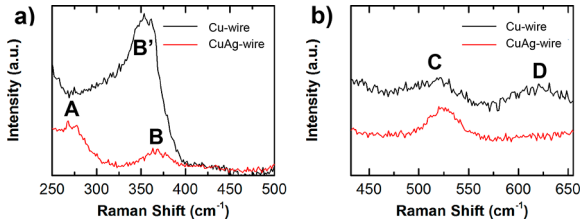

Figure 7. *In situ* Raman spectra of Cu wire and CuAg wire in a flow cell while both electrolyte 1 M KOH and CO_2 are flowing through the electrode surface at a potential of −0.7 V vs RHE in two regions: (a) Cu−CO stretch and (b) Cu−O stretch.

consisting of 1 M KOH flowing at a rate of 20 mL/min over the Cu or CuAg catalyst supported on carbon paper while CO_2 is flowing at a rate of 4 SCCM and the sample is held at a potential of −0.7 V vs RHE. We measured the pH of the electrolyte before and after flowing through the cell and found no change, showing that the interaction of CO_2 with KOH was minimal in this experimental configuration.

Figure 7a shows the-low frequency region. In the case of the Cu wire catalyst, one band is observed at 356 cm^{-1} (Band B′) associated with the Cu−CO stretch.[52] In contrast, Raman spectra obtained from the CuAg wire catalyst exhibit two bands, one at 260 cm^{-1} (Band A) and another at 369 cm^{-1} (Band B). Band A is associated with the so-called frustrated rotation (or Cu−C−O bend) of CO bound to the Cu surface. Band B′ is similar to band B from the Cu wire catalyst, but shifted by 13 cm^{-1}. Band A has been observed in SERS obtained from Cu surfaces at low temperature.[52] Under these low temperature UHV conditions, Band A is prominent in samples where the CO concentration on the Cu surface is relatively low. By way of contrast, as the CO concentration is increased, the intensity of band B is found to increase at the expense of band A.[52] This prior work suggests that the appearance of band A in the CuAg wire catalyst is associated with a surface exhibiting a sparser

DOI: 10.1021/jacs.8b01868
J. Am. Chem. Soc. 2018, 140, 5791−5797

coverage of CO relative to the Cu wire catalyst. Interestingly, the Cu wire catalyst generates more CO at this potential relative to CuAg wire catalyst. Unfortunately, no CO stretching modes in the 2100 cm^{-1} region were observed in either sample.

Figure 7b shows Raman spectra obtained simultaneously with those in Figure 7a. The Cu wire catalyst exhibits two bands at 526 cm^{-1} (band C) and 624 cm^{-1} (band D). Band C is associated with the Cu−O stretch in a Cu(I)oxide while band D is associated with Cu(II)oxide.[53] By way of contrast, the CuAg wire catalyst exhibits only band C. Thus, the presence of Cu_2O is associated with the CuAg wire catalyst.

The oxidation state of Cu electrodes has been shown to have a significant effect on product selectivity during CO_2 electroreduction. Cu is widely accepted to produce CO and HCOOH as the main products at low overpotentials and CH_4 or C_2H_4 at higher overpotentials. On the other hand, Cu_2O is mostly reported to yield CH_3OH with high efficiency.[54,55] However, the catalytic activity of Cu_2O decreases quickly due to the decomposition of Cu_2O to Cu,[14] and methanol is formed only during the reduction of these oxide films. After the reaction, both Cu(I) and Cu(II) are present on the electrode, as measured by *ex situ* Auger.[55] These data are consistent with our *in situ* Raman data for the Cu wire electrode, which show the presence of both Cu(I) and Cu(II) oxides and is also less effective at producing C_2H_4 relative to CuAg wire.

The CuAg wire electrode exhibits only Cu_2O. The presence of only this oxide is consistent with other reports where the presence of Cu_2O yields enhancement in CO and C_2H_4 production efficiency.[14,15,56] It is also reported that the orientation of electrodeposited Cu_2O ([110], [111], and [100]) has only a minor effect on product selectivity.[14] However, the initial oxide thickness strongly influences the selectivity of the electrocatalytic process. This behavior was explained by differences in surface roughness and local pH at each sample exhibiting different oxide thickness. Prior work examining the effect of different pH values on ethylene selectivity found that high pH yielded greater C_2H_4 production.[13,57]

While the Cu wire electrode exhibits both Cu_2O and CuO, no evidence of CuO, only Cu_2O was found on the CuAg wire electrode. This result is consistent with other reports where the presence of Ag significantly improve the resistance to oxidation of CuAg nanoparticles compared to pure Cu nanoparticles; in particular, less CuO was observed in CuAg samples than in Cu samples.[58] The XPS data used to make this conclusion can only distinguish between Cu and CuO, but cannot distinguish between Cu and Cu_2O. Thus, no comparison of the relative Cu_2O content in Cu and CuAg samples has been reported.

In this work, both Raman and EXAFS suggest that the CuAg wire electrode exhibits enhanced formation of Cu_2O and little adsorbed CO. We suggest that the presence of Ag helps promote the formation of Cu_2O on the Cu surface. This phenomenon can be explained by using two related thermodynamic arguments. First, the formation enthalpies of Cu_2O (−169 kJ/mol) and Ag_2O (−31.1 kJ/mol) are substantially different, so any Ag oxide that may form during oxygen exposure will be promptly reduced by the neighboring Cu.[59] Second, Ag has a higher redox potential than Cu and can accept electrons from Cu. Thus, Cu atoms in the CuAg samples will exhibit a slightly more positive charge that promotes formation of Cu_2O relative to pure Cu. However, voltammetry associated with Cu oxidation and reduction in alkaline alone,[60,61] and in CO_2 reduction show that there are no explicit oxidation or reduction waves associated with Cu oxidation at the negative potentials considered here.

The GC data show that the presence of Ag in the form of a CuAg alloy in the CuAg wire electrode significantly improves the activity and selectivity of the CO_2 electroreduction reaction toward C_2H_4 production relative to the segregated Ag in the CuAg poly sample and pure Cu. There are two possible reasons for this effect. First, as discussed above, Ag promotes the formation of Cu_2O in CuAg electrode, leading to enhancement in CO and C_2H_4 production efficiency. Second, Ag is an active promoter that forms more CO and could help generate a higher flux of CO, so that neighboring Cu may have more opportunity to participate in coupling.[62,63] When the Ag content is too small (3% of Ag was tested), the formation of C_2H_4 decreases especially at high reduction potential where large amount of CO is required to form C_2H_4 (Figure S2). When Ag content is larger (9% of Ag was tested), the stress inherent in CuAg begins to drive Ag atoms segregate into islands (Figure S2).[59] Thus, when too much Ag is present in CuAg samples, the main product of CO_2 reduction reaction will be CO.[20]

4. CONCLUSION

In this work, we have developed a facile method to co-electrodeposit high surface area CuAg alloys, resulting from the inhibition of nucleation through the presence of an additive, DAT. EXAFS data demonstrated that while Cu and Ag atoms in CuAg poly samples that are electrodeposited without DAT are completely segregated, those in CuAg wire samples are more homogeneously mixed. Flow electrolyzer experiments showed that the CuAg wire samples exhibit much higher activity and selectivity for the electroreduction CO_2 to C_2 products (C_2H_4 and C_2H_5OH) in comparison to the CuAg poly and Cu wire samples.

■ ASSOCIATED CONTENT

Supporting Information

The Supporting Information is available free of charge on the ACS Publications website at DOI: 10.1021/jacs.8b01868.

SEM images and electrochemical performance data for CuAg wire with 3, 6, and 9% Ag loading, including Figures S1−S5 and Table S1 (PDF)

■ AUTHOR INFORMATION

Corresponding Author

*agewirth@illinois.edu

ORCID

Tim T. Fister: 0000-0001-6537-6170
Anatoly I. Frenkel: 0000-0002-5451-1207
Paul J. A. Kenis: 0000-0001-7348-0381
Andrew A. Gewirth: 0000-0003-4400-9907

Notes

The authors declare no competing financial interest.

■ ACKNOWLEDGMENTS

This work was supported by the NSF (Grant CHE-1309731) which is gratefully acknowledged. We also acknowledge the International Institute for Carbon Neutral Energy Research (WPI-I2CNER), which is sponsored by the World Premier International Research Center Initiative (WPI) of MEXT in Japan. A.I.F. and J.T. acknowledge the NSF (Grant CHE-

DOI: 10.1021/jacs.8b01868
J. Am. Chem. Soc. 2018, 140, 5791−5797

1726321). T.T.H.H. acknowledges the Graduate University of Science and Technology (grant number GUST.STS.ĐT2017-HH09) for support.

REFERENCES

(1) Ussiri, D. A.; Lal, R. *Introduction to Global Carbon Cycling: An Overview of the Global Carbon Cycle. In Carbon Sequestration for Climate Change Mitigation and Adaptation*; Springer: Cham, Switzerland, 2017.
(2) Hansen, J.; Kharecha, P.; Sato, M.; Masson-Delmotte, V.; Ackerman, F.; Beerling, D. J.; Hearty, P. J.; Hoegh-Guldberg, O.; Hsu, S.-L.; Parmesan, C.; Rockstrom, J.; Rohling, E. J.; Sachs, J.; Smith, P.; Steffen, K.; Van Susteren, L.; von Schuckmann, K.; Zachos, J. C. *PLoS One* **2013**, *8*, e81648.
(3) Whipple, D. T.; Kenis, P. J. A. *J. Phys. Chem. Lett.* **2010**, *1*, 3451.
(4) Yang, H.; Xu, Z.; Fan, M.; Gupta, R.; Slimane, R. B.; Bland, A. E.; Wright, I. *J. Environ. Sci. (Beijing, China)* **2008**, *20*, 14.
(5) Appel, A. M.; Bercaw, J. E.; Bocarsly, A. B.; Dobbek, H.; DuBois, D. L.; Dupuis, M.; Ferry, J. G.; Fujita, E.; Hille, R.; Kenis, P. J. A.; Kerfeld, C. A.; Morris, R. H.; Peden, C. H. F.; Portis, A. R.; Ragsdale, S. W.; Rauchfuss, T. B.; Reek, J. N. H.; Seefeldt, L. C.; Thauer, R. K.; Waldrop, G. L. *Chem. Rev.* **2013**, *113*, 6621.
(6) Olah, G. A.; Prakash, G. K. S.; Goeppert, A. *J. Am. Chem. Soc.* **2011**, *133*, 12881.
(7) Costentin, C.; Robert, M.; Saveant, J.-M. *Chem. Soc. Rev.* **2013**, *42*, 2423.
(8) Lim, R. J.; Xie, M. S.; Sk, M. A.; Lee, J. M.; Fisher, A.; Wang, X.; Lim, K. H. *Catal. Today* **2014**, *233*, 169.
(9) Kortlever, R.; Shen, J.; Schouten, K. J. P.; Calle-Vallejo, F.; Koper, M. T. M. *J. Phys. Chem. Lett.* **2015**, *6*, 4073.
(10) Hori, Y. In *Modern Aspects of Electrochemistry*; Vayenas, C. G., White, R. E., Gamboa-Aldeco, M. E., Eds.; Springer: New York, 2008; p 89.
(11) Tang, W.; Peterson, A. A.; Varela, A. S.; Jovanov, Z. P.; Bech, L.; Durand, W. J.; Dahl, S.; Norskov, J. K.; Chorkendorff, I. *Phys. Chem. Chem. Phys.* **2012**, *14*, 76.
(12) Kas, R.; Hummadi, K. K.; Kortlever, R.; de Wit, P.; Milbrat, A.; Luiten-Olieman, M. W. J.; Benes, N. E.; Koper, M. T. M.; Mul, G. *Nat. Commun.* **2016**, *7*, 10748.
(13) Ma, S. C.; Sadakiyo, M.; Luo, R.; Heima, M.; Yamauchi, M.; Kenis, P. J. A. *J. Power Sources* **2016**, *301*, 219.
(14) Kas, R.; Kortlever, R.; Milbrat, A.; Koper, M. T. M.; Mul, G.; Baltrusaitis, J. *Phys. Chem. Chem. Phys.* **2014**, *16*, 12194.
(15) Li, C. W.; Kanan, M. W. *J. Am. Chem. Soc.* **2012**, *134*, 7231.
(16) Manthiram, K.; Beberwyck, B. J.; Alivisatos, A. P. *J. Am. Chem. Soc.* **2014**, *136*, 13319.
(17) Mistry, H.; Varela, A. S.; Bonifacio, C. S.; Zegkinoglou, I.; Sinev, I.; Choi, Y. W.; Kisslinger, K.; Stach, E. A.; Yang, J. C.; Strasser, P.; Cuenya, B. R. *Nat. Commun.* **2016**, *7*, 12123.
(18) Ma, M.; Djanashvili, K.; Smith, W. A. *Angew. Chem., Int. Ed.* **2016**, *55*, 6680.
(19) Ren, D.; Ang, B. S.-H.; Yeo, B. S. *ACS Catal.* **2016**, *6*, 8239.
(20) Choi, J.; Kim, M. J.; Ahn, S. H.; Choi, I.; Jang, J. H.; Ham, Y. S.; Kim, J. J.; Kim, S. K. *Chem. Eng. J.* **2016**, *299*, 37.
(21) Kim, D.; Resasco, J.; Yu, Y.; Asiri, A. M.; Yang, P. D. *Nat. Commun.* **2014**, *5*, 4948.
(22) Christophe, J.; Doneux, T.; Buess-Herman, C. *Electrocatalysis* **2012**, *3*, 139.
(23) Dutta, A.; Rahaman, M.; Mohos, M.; Zanetti, A.; Broekmann, P. *ACS Catal.* **2017**, *7*, 5431.
(24) Reller, C.; Krause, R.; Volkova, E.; Schmid, B.; Neubauer, S.; Rucki, A.; Schuster, M.; Schmid, G. *Adv. Energy Mater.* **2017**, *7*, 1602114.
(25) Schouten, K. J. P.; Qin, Z. S.; Gallent, E. P.; Koper, M. T. M. *J. Am. Chem. Soc.* **2012**, *134*, 9864.
(26) Hori, Y.; Takahashi, I.; Koga, O.; Hoshi, N. *J. Mol. Catal. A: Chem.* **2003**, *199*, 39.
(27) Watanabe, M.; Shibata, M.; Kato, A.; Azuma, M.; Sakata, T. *J. Electrochem. Soc.* **1991**, *138*, 3382.
(28) Clark, E. L.; Hahn, C.; Jaramillo, T. F.; Bell, A. T. *J. Am. Chem. Soc.* **2017**, *139*, 15848.
(29) Verma, S.; Kim, B.; Jhong, H. R. M.; Ma, S.; Kenis, P. J. A. *ChemSusChem* **2016**, *9*, 1972.
(30) Martin, A. J.; Larrazabal, G. O.; Perez-Ramirez, J. *Green Chem.* **2015**, *17*, 5114.
(31) Larrazabal, G. O.; Martin, A. J.; Perez-Ramirez, J. *J. Phys. Chem. Lett.* **2017**, *8*, 3933.
(32) Hoang, T. T. H.; Ma, S. C.; Gold, J. I.; Kenis, P. J. A.; Gewirth, A. A. *ACS Catal.* **2017**, *7*, 3313.
(33) Wu, G. Y.; Bae, S. E.; Gewirth, A. A.; Gray, J.; Zhu, X. D.; Moffat, T. P.; Schwarzacher, W. *Surf. Sci.* **2007**, *601*, 1886.
(34) Schultz, Z. D.; Feng, Z. V.; Biggin, M. E.; Gewirth, A. A. *J. Electrochem. Soc.* **2006**, *153*, C97.
(35) Schlesinger, M.; Paunovic, M. *Modern Electroplating*, 5th ed.; Wiley: Hoboken, NJ, 2010.
(36) Hoang, T. T. H.; Gewirth, A. A. *ACS Catal.* **2016**, *6*, 1159.
(37) Liang, D.; Shao, W.; Zangari, G. *J. Electrochem. Soc.* **2016**, *163*, D40.
(38) Biesinger, M. C.; Lau, L. W. M.; Gerson, A. R.; Smart, R. S. C. *Appl. Surf. Sci.* **2010**, *257*, 887.
(39) Zhu, C. Q.; Osherov, A.; Panzer, M. J. *Electrochim. Acta* **2013**, *111*, 771.
(40) Yin, M.; Wu, C. K.; Lou, Y. B.; Burda, C.; Koberstein, J. T.; Zhu, Y. M.; O'Brien, S. *J. Am. Chem. Soc.* **2005**, *127*, 9506.
(41) Yu, L.; Akolkar, R. *J. Electrochem. Soc.* **2016**, *163*, D247.
(42) Sharma, A.; Varshney, M.; Park, J.; Ha, T. K.; Chae, K. H.; Shin, H. J. *RSC Adv.* **2015**, *5*, 21762.
(43) Kuhl, K. P.; Cave, E. R.; Abram, D. N.; Jaramillo, T. F. *Energy Environ. Sci.* **2012**, *5*, 7050.
(44) Schouten, K. J. P.; Kwon, Y.; van der Ham, C. J. M.; Qin, Z.; Koper, M. T. M. *Chem. Sci.* **2011**, *2*, 1902.
(45) Montoya, J. H.; Shi, C.; Chan, K.; Norskov, J. K. *J. Phys. Chem. Lett.* **2015**, *6*, 2032.
(46) Ren, D.; Deng, Y. L.; Handoko, A. D.; Chen, C. S.; Malkhandi, S.; Yeo, B. S. *ACS Catal.* **2015**, *5*, 2814.
(47) Durand, W. J.; Peterson, A. A.; Studt, F.; Abild-Pedersen, F.; Norskov, J. K. *Surf. Sci.* **2011**, *605*, 1354.
(48) Hori, Y.; Takahashi, I.; Koga, O.; Hoshi, N. *J. Mol. Catal. A: Chem.* **2003**, *199*, 39.
(49) Clark, E. L.; Hahn, C.; Jaramillo, T. F.; Bell, A. T. *J. Am. Chem. Soc.* **2017**, *139*, 15848.
(50) Yoon, Y.; Hall, A. S.; Surendranath, Y. *Angew. Chem., Int. Ed.* **2016**, *55*, 15282.
(51) Hall, A. S.; Yoon, Y.; Wuttig, A.; Surendranath, Y. *J. Am. Chem. Soc.* **2015**, *137*, 14834.
(52) Akemann, W.; Otto, A. *Surf. Sci.* **1993**, *287-288*, 104.
(53) Debbichi, L.; de Lucas, M. C. M.; Pierson, J. F.; Kruger, P. *J. Phys. Chem. C* **2012**, *116*, 10232.
(54) Le, M.; Ren, M.; Zhang, Z.; Sprunger, P. T.; Kurtz, R. L.; Flake, J. C. *J. Electrochem. Soc.* **2011**, *158*, E45.
(55) Frese, K. W. *J. Electrochem. Soc.* **1991**, *138*, 3338.
(56) Bugayong, J.; Griffin, G. L. *ECS Trans.* **2013**, *58*, 81.
(57) Jhong, H. R.; Ma, S. C.; Kenis, P. J. A. *Curr. Opin. Chem. Eng.* **2013**, *2*, 191.
(58) Kim, N. R.; Shin, K.; Jung, I.; Shim, M.; Lee, H. M. *J. Phys. Chem. C* **2014**, *118*, 26324.
(59) Hirsimaki, M.; Lampimaki, M.; Lahtonen, K.; Chorkendorff, I.; Valden, M. *Surf. Sci.* **2005**, *583*, 157.
(60) Kang, M. C.; Gewirth, A. A. *J. Phys. Chem. B* **2002**, *106*, 12211.
(61) Kunze, J.; Maurice, V.; Klein, L. H.; Strehblow, H. H.; Marcus, P. *J. Phys. Chem. B* **2001**, *105*, 4263.
(62) Peterson, A. A.; Norskov, J. K. *J. Phys. Chem. Lett.* **2012**, *3*, 251.
(63) Shi, C.; Hansen, H. A.; Lausche, A. C.; Norskov, J. K. *Phys. Chem. Chem. Phys.* **2014**, *16*, 4720.

DOI: 10.1021/jacs.8b01868
J. Am. Chem. Soc. 2018, 140, 5791−5797